Influence of Injector Location on Part-Load Performance Characteristics of Natural Gas Direct-Injection in a Spark Ignition Engine

Author, co-author (Do NOT enter this information. It will be pulled from participant tab in MyTechZone)

Affiliation (Do NOT enter this information. It will be pulled from participant tab in MyTechZone)

ABSTRACT

Interest in natural gas as an alternative fuel source to petroleum fuels for light-duty vehicle applications has increased due to its domestic availability and stable price compared to gasoline. With its higher hydrogen-to-carbon ratio, natural gas has the potential to reduce engine out carbon dioxide emissions, which has shown to be a strong greenhouse gas contributor. For part-load conditions, the lower flame speeds of natural gas can lead to an increased duration in the inflammation process with traditional port-injection. Direct-injection of natural gas can increase in-cylinder turbulence and has the potential to reduce problems typically associated with port-injection of natural gas, such as lower flame speeds and poor dilution tolerance.

A study was designed and executed to investigate the effects of direct-injection of natural gas at part-load conditions. Steady-state tests were performed on a single-cylinder research engine representative of current gasoline direct-injection engines. Tests were performed with direct-injection in the central and side location. The start of injection was varied under stoichiometric conditions in order to study the effects on the mixture formation process. In addition, exhaust gas recirculation was introduced at select conditions in order to investigate the dilution tolerance. Relevant combustion metrics were then analyzed for each scenario.

Experimental results suggest that regardless of the injector location, varying the start of injection has a strong impact on the mixture formation process. Delaying the start of injection from 300 to 120°CA BTDC can reduce the early flame development process by nearly 15°CA. While injecting into the cylinder after the intake valves have closed has shown to produce the fastest combustion process, this does not necessarily lead to the highest efficiency, due to increases in pumping and wall heat losses. When comparing the two injection configurations, the side location shows the best performance in terms of combustion metrics and efficiencies. For both systems, part-load dilution tolerance is affected by the injection timing, due to the induced turbulence from the gaseous injection event. CFD simulation results have shown that there is a fundamental difference in how the two injection locations affect the mixture formation process. Delayed injection timing increases the turbulence level in the cylinder at the time of the spark, but reduces the available time for proper mixing. Side injection delivers a gaseous jet that interacts more effectively with the intake induced flow field, and this improves the engine performance in terms of efficiency.

INTRODUCTION

The use of natural gas (NG) as a transportation fuel can be traced back to World War I and World War II when it was used out of necessity due to gasoline shortages [1]. Due to increasing availability and production of NG in the U.S., interest in NG has once again increased. Future production forecasts show NG production to continue to increase [2]. In addition, the cost of NG on a gasoline gallon equivalent (GGE) basis has remained stable over the last decade, as shown in Figure 1, compared to the much more volatile gasoline, diesel, and E85.
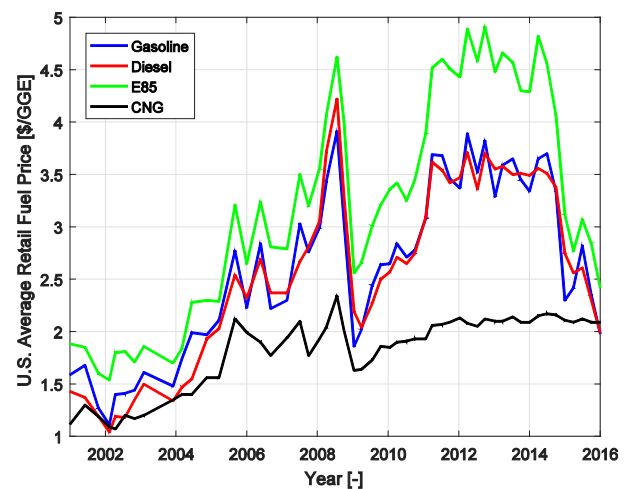

Figure 1: Marketed U.S. Natural Gas Production [3]

NG retrofit kits have gained popularity due to the domestic availability of gas, as well as the ability for NG consumption to reduce CO_2 emissions [4,5,6]. A common method is to introduce NG into the engine by replacing or adding a secondary port-fuel NG injector [7,8]. However, due to the lower flame speeds of natural gas, the length of the combustion process can increase significantly and at the same time decrease dilution tolerance when using port-injection of NG [6].

The availability of production level NG vehicles has also increased in recent years. Anderson et al. performed vehicle level tests on a chassis dynamometer over several drive cycles with a production NG vehicle and its gasoline counterpart [9]. Despite having a higher compression ratio, the NG vehicle yielded 3-9% lower fuel economy than the gasoline comparator. In addition to a 21% loss in peak power, the external-EGR loop was removed from the factory due to the lower dilution tolerance of NG. It was

concluded that manufacturing an engine specifically for natural gas operation, with features such as NG direct-injection (DI) and increased charge motion, could meet or exceed efficiencies of current state-of-the-art gasoline engines.

While downsized boosted gasoline direct-injection (GDI) engines have become increasingly popular, there is also increased research involving NG DI. Husted et al has shown that under low engine speeds, NG port-fuel injection can lead to a loss in low end torque, up to 30% relative to GDI operation [10]. With NG DI, up to two-thirds of the lost engine torque can be made up for by maintaining combustion phasing for peak efficiency. In addition, where GDI operation may become knock limited, NG DI allows for optimal combustion phasing while minimizing the chance of engine knock due to the higher knock resistance of NG.

Previous works of the authors have investigated the effects of gasoline and NG port-fuel injection and central NG DI at a part-load and full load condition [6]. Regardless of the injection system, similar part-load efficiencies were realized for gasoline and NG. Yet, while the effects of injection timing were minimal for the port-fuel injection systems, varying the injection timing for NG DI played a crucial role in influencing the early flame development process, as well as impacting the efficiency. In addition, NG DI allowed for a 10% load improvement at full load conditions relative to gasoline and NG port-fuel injection strategies. NG also allowed for higher efficiencies at full load relative to gasoline due to its higher knock resistance.

The purpose of this study is to investigate the performance, efficiency, and emissions characteristics of NG DI. In addition, the interactions of two different injector locations and their influence on the combustion process will be analyzed. Steady-state tests were conducted at part-load to study the effects of a gaseous injection event on the combustion process, as well as exhaust gas recirculation (EGR) dilution tolerance. Computational fluid dynamics (CFD) results will also be analyzed to further help explain the experimental results.

EXPERIMENTAL SETUP

Steady-state tests were conducted on a single-cylinder research engine, equipped for both centrally and side mounted NG DI. This engine configuration is representative of modern GDI engines, with specifications shown in Table 1. The cylinder head featured a 40° pent roof combustion chamber with a centrally mounted spark plug.

Table 1: Engine geometry

Displaced volume	0.6264 L
Stroke	100.6 mm
Bore	89.04 mm
Compression ratio	10.5:1
Number of Valves	4
Spark Plug	NGK, 0.7mm gap
Tumble ratio	0.6

High speed crank angle resolved cylinder pressure data were recorded using an AVL GU21C transducer and AVL 365X crank angle encoder with a 0.5°CA physical resolution. Combustion air was supplied to the engine from an Atlas Copco air compressor; throttled conditions were achieved using a Parker pilot operated regulator in the intake stream.

A cooled high pressure EGR loop was installed in the test cell, using an automotive style EGR valve to control external EGR flow and temperature. Engine coolant was circulated through the EGR cooler, held at 85°C. The cooled EGR was introduced before the intake surge tank to ensure homogenous distribution in the intake charge. CO_2 concentrations in ambient air were sampled twice daily to ensure representative EGR rates. EGR rates were calculated using Equation 1, sampling CO_2 emissions from the intake and exhaust stream. Raw emissions were sampled using a Pierburg AMA2000 emissions bench.

$$EGR = \frac{CO_{2_{intake}} - CO_{2_{ambient}}}{CO_{2_{exhaust}} - CO_{2_{ambient}}} \qquad (1)$$

A conventional transistorized coil ignition (TCI) system was used for all tests performed. This coil is representative of coils currently implemented on GDI engines in the market, with a nominal energy level of 75 mJ.

Unique to this study is usage of a fourth generation natural gas DI injector, supplied by Delphi [11]. This injector features an outward-opening valve, with maximum allowable injection pressure of up to 16 bar absolute. In order to maintain critical flow, the minimum injection pressure is 8 bar absolute. This injector allows for injection events to occur after intake valves close, which has shown to improve low speed high load performance over gaseous port-fuel injection strategies [4]. Figure 2 shows a schematic of the combustion chamber with central and side mounted DI injectors. As can be seen, the side injector injects along the direction of the intake charge motion, while the central injector injects directly towards the piston. Literature has shown that it is possible for injection timings between 320-260°CA BTDC can lead to back-flow of NG into the intake manifold [12].
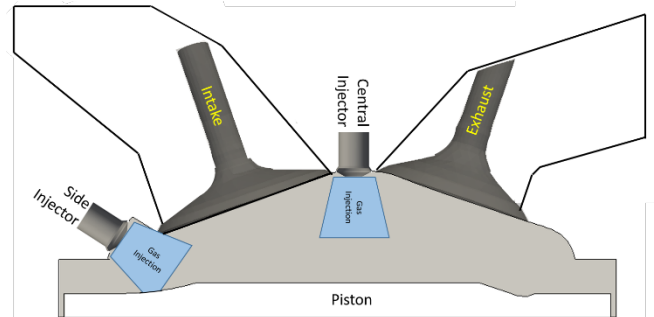

Figure 2: Combustion Chamber Schematic featuring Central and Side NG DI Injectors

Figure 3 shows the valve lift profiles as a function of crank angle, with markers for exhaust valve closure (EVC), intake valve closure (IVC), exhaust valve open (EVO), and intake valve open

(IVO). As seen, any injection timing after -140°CA ATDC is a closed valve event for DI. Injecting while the intake valves are open can assist in reducing pumping losses, especially at part-load conditions. As previously mentioned, some injection timings may lead to back-flow of natural gas into the intake manifold. As shown in Figure 3, for this given test setup, an injection timing occurring between 360 to 140°CA BTDC could lead to back-flow. If this occurs, the natural gas in the intake manifold would be reintroduced during the next combustion event.
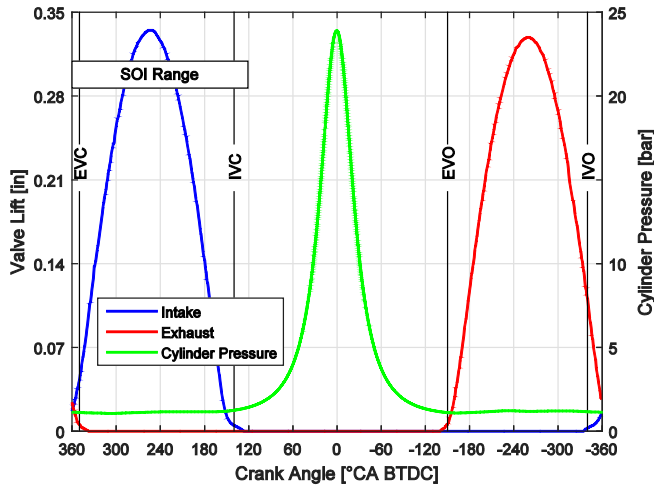
Figure 3: Valve lift profiles as a function of crank angle

The composition of natural gas will vary based off of the regional location as well as time of the year [13]. It was therefore decided to perform tests with custom blends of compressed natural gas (CNG) from a regional distributor rather than pipeline natural gas, in order to keep composition of the gas constant. Table 2 shows the speciated composition of the CNG, as well as other relevant parameters. Methane number (MN) was chosen to evaluate the knock resistance of CNG, as opposed to using the motor octane number (MON). Test bounds setup to determine MON are designed for fuels with a maximum MON~120 and generally are not suited for fuels with very high knock resistance [14,15]. The methane number is a function of the hydrogen-to-carbon ratio, with pure methane having a reference number of 100 [16]. Heavier hydrocarbons such as ethane and propane will lower the value of the methane number.

Table 2: Gaseous Fuel Specifications

CH4, C2H6, CO2, N2 [mol%]	94, 3, 2, 1
MN [-]	90.7
LHV [MJ/kg]	46.93
AFRSTOICH [-]	16.2

EXPERIMENTAL APPROACH

Steady-state engine testing was performed at a single speed and load condition, summarized in Table 3. Every data point plotted in subsequent figures represent three averaged data points collected over 30 seconds at 5 Hz. Stoichiometric operation was maintained for all operating points. Closed-loop control was used through the use of a Motec M800 engine control unit (ECU). Start of injection (SOI) for DI operation was limited due to increasing cylinder pressure during the early compression stroke and a need to maintain sufficient time between the end of injection (EOI) and spark timing. SOI timing with DI during the gas exchange phase was limited to 360°CA BTDC to avoid excessive short circuiting of natural gas through the open exhaust valves. In addition, injection pressure was held constant at 16 bar absolute for all conditions. Maximum brake torque (MBT) timing was maintained for all test conditions; spark timing was adjusted for each condition to target a mass fraction burned (MFB) 50% location of 8°CA ATDC.

Table 3: Experimental test conditions

Engine Speed [rpm]	1500
IMEP$_{NET}$ [bar]	5.6
SOI DI [°CA BTDC fired]	Sweep, 120-360
Injection Pressure [barA]	16

COMBUSTION METRICS

Several combustion metrics are used to analyze the experimental results. The flame development angle, shown in Equation 2, is defined as the crank angle duration from the time of the spark event, until a fraction of the fuel energy has been released; MFB10% has been chosen for this study [17].

$$Flame\ Development\ Angle = MFB10\% - Spark \qquad (2)$$

The combustion duration is used to describe the overall burning process, defined in Equation 3 as the crank angle duration from MFB10% to MFB90% [17].

$$Combustion\ Duration = MFB90\% - MFB10\% \qquad (3)$$

Cyclic variability was also of interest, and was measured using the coefficient of variance of the indicated net mean effective pressure (COV$_{IMEP}$). The COV$_{IMEP}$ is defined in Equation 4 as the standard deviation of IMEP divided by the mean IMEP. A 3% limit was imposed for stable engine operation and all high speed data were analyzed over 375 cycles.

$$COV_{IMEP} = \frac{\sigma_{IMEP}}{\mu_{IMEP}} \qquad (4)$$

Combustion efficiency was also analyzed, defined in Equation 5, as the amount of fuel energy supplied which is released during the combustion process. For this analysis only carbon monoxide and total hydrocarbons were considered [17]. Analyzing the combustion efficiency is of particular interest when performing EGR sweeps.

$$\eta_c = 1 - \frac{\Sigma_i x_i Q_{HVi}}{[\dot{m}_f/(\dot{m}_a + \dot{m}_f)]Q_{LHVf}} \qquad (5)$$

RESULTS
INFLUENCE OF SOI

Figure 4 shows the relevant combustion metrics for central and side DI without EGR. As seen, the net indicated thermal efficiency (ITE) varies considerably with changing start of

injection (SOI). Despite the advanced injection timing, ITE reaches a minimum of 34.6 and 35.2% at SOI 300°CA BTDC for central and side DI. Central and side DI reach a maximum ITE of 35.6% and 35.8%, respectively, at 240°CA BTDC. As the start of injection is delayed closer to top dead center (TDC) after maximum ITE, the ITE begins to decrease. This can likely be attributed to some level of in-cylinder stratification being achieved, as well as positive charge motion from the NG DI injection event increasing wall heat transfer [4]. Furthermore, the gas exchange work increases as the SOI is delayed due to the engine aspirating more air. For all SOI conditions, the COV$_{IMEP}$ was below the 3% limit for both central and side DI.
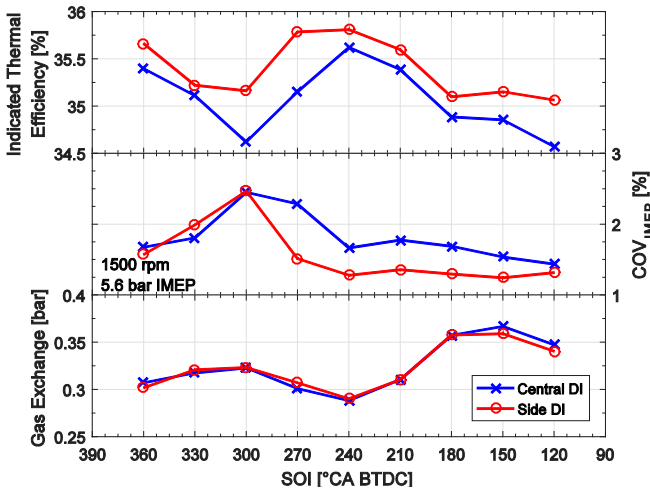
Figure 4: ITE, COV$_{IMEP}$ and Gas Exchange for Central and Side NG DI as a function of SOI

The flame development angle and combustion duration also show a strong dependence on the SOI, shown in Figure 5. The longest flame development angle and combustion duration occur at 300°CA BTDC, corresponding to the location of lowest ITE and highest COV$_{IMEP}$. As the SOI is delayed closer to TDC, the flame development angle and combustion duration begin to decrease. It is interesting to note, changing the SOI between 270 and 120°CA BTDC for side DI has less of an impact than for central DI, indicating there is a different interaction between the gaseous injection event and intake flow for the two injection systems. There is also a distinct difference in flame development angle and combustion duration for a given SOI value in this range. For the instance of SOI 240°CA BTDC, there is a 9 and 4°CA difference in flame development angle and combustion duration. At the same time, while injecting at SOI 120°CA BTDC yields the shortest overall combustion process for both injection systems, it does not yield the highest efficiency. It could be that the earlier injection helps to compound the in-cylinder turbulence that is already introduced with the intake system. It is shown in the literature that increasing in-cylinder turbulence can lead to an increase in rate of development and propagation for the combustion process [17].
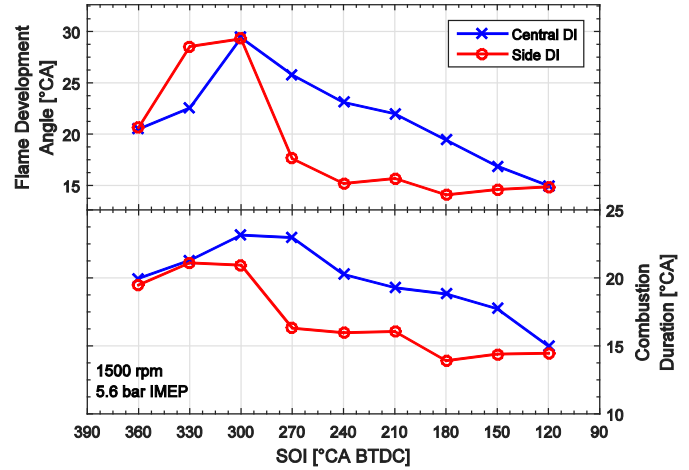

Figure 5: Flame Development Angle and Combustion Duration for Central and Side NG DI as a function of SOI

To provide further insight into the observed trends, the rate of heat release (ROHR) was analyzed for the three nominal SOI values, for both central and side DI, shown in Figure 6. SOI 300°CA BTDC was chosen as this has shown to be a condition with poor mixing, SOI 240°CA BTDC which coincides with maximum ITE and SOI 120°CA BTDC because it is a closed valve injection event. In Figure 6, each subplot contains all six ROHR curves for central and side DI. The colored pairs for each subplot correspond for the given SOI analyzed, as shown on the y-axis. Markers are used to differentiate between injection systems. As can be seen, both central and side DI at SOI 300°CA BTDC have the slowest ROHR, which is consistent with the longest flame development angle and combustion duration. At the same time, the fastest ROHR occurred for central and side DI at SOI 120°CA BTDC, corresponding to the shortest flame development angle and combustion duration. The most interesting difference is between central and side DI at SOI 240°CA BTDC. Despite injecting at the same time, there is a distinct difference in the ROHR, indicating there is a fundamental difference with how the gaseous injection event interacts with the intake flow. For reference, at SOI 120°CA BTDC the injection duration for central and side DI is 25°CA, with there being an 80°CA duration between the EOI and spark timing. However, a larger difference occurs at SOI 240°CA BTDC where there is a 190 and 200°CA interval between EOI and spark timing for central and side DI, respectively, for the same injection duration. This is interesting, because despite the longer time for mixing at SOI 240°CA BTDC, side DI results in a heat release rate similar to that of 120°CA BTDC. This is possibly due to more favorable conditions in the near spark region for side than central DI.
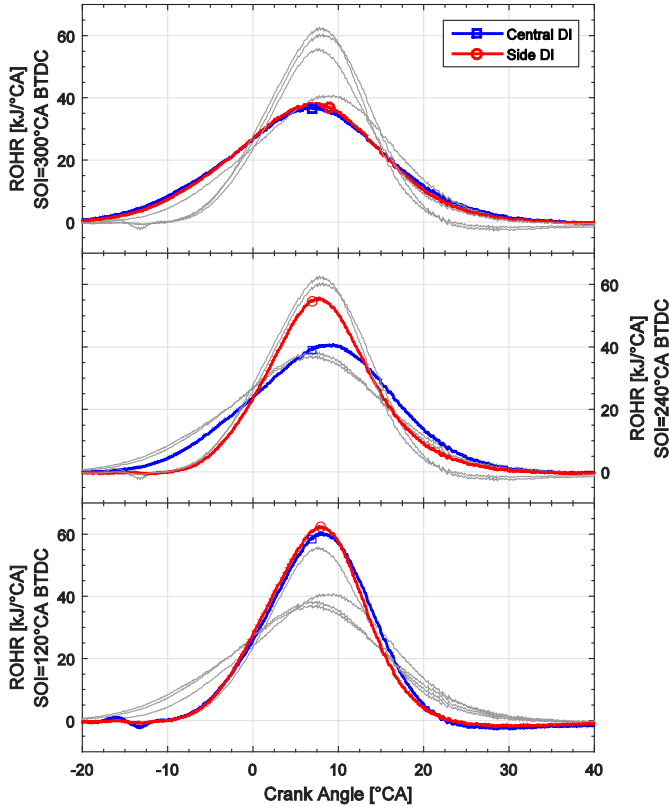
Figure 6: Rate of Heat Release for Central and Side DI

Figure 7 shows indicated specific emissions as a function of SOI for central and side DI. The greatest change in indicated specific hydrocarbon (iSHC) emissions is for side DI, with a minimum of 1.33 g/kWhr at SOI 330°CA BTDC to a maximum of 2g/kWhr at 120°CA BTDC. With the exception of 360°CA BTDC, central DI stayed at or below 1.5g/kWhr for all operating conditions. The same general trend for iSCO occurred for central and side DI. iSCO emissions reached a minimum for SOI 240°CA BTDC for both central and side DI, and continued to increase as the SOI was delayed closer to TDC. It is also interesting to note that combustion efficiency is better for side DI for most of the injection timings, but converges at the extremes of the SOI range. The low level of combustion efficiency at SOI 300°CA BTDC for central and side DI may be due to unfavorable in-cylinder conditions at the time of spark. The general increase in iSHC and iSCO and decrease in combustion efficiency after SOI 240°CA BTDC can be attributed to a decrease in the time from the EOI to the time of spark, decreasing the level of homogeneity. Focusing on SOI 240°CA BTDC, it can be seen iSHC emissions are similar, yet iSCO are nearly double comparing central to side DI. In addition to the lowest gas exchange work seen in Figure 4, it can be concluded there is an optimal mixing condition for this given SOI. In addition, given the factor of two difference in iSCO emissions, there is likely a different flow-field interaction for central and side DI.
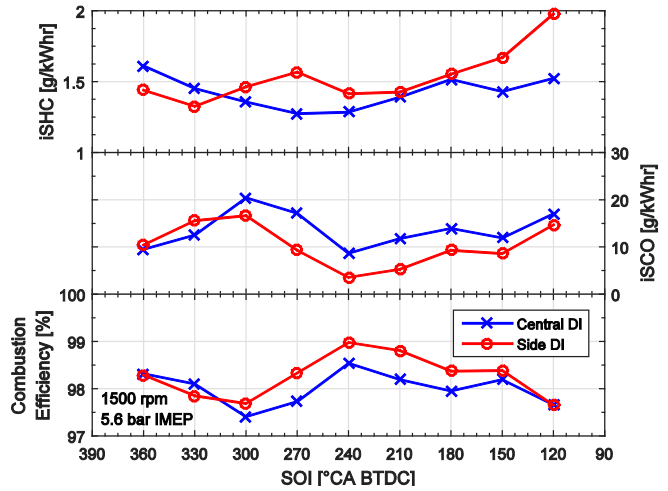

Figure 7: Specific HC and CO Emissions and Combustion Efficiency as a function of SOI for Central and Side DI

Figure 8 shows indicated specific carbon dioxide (iSCO$_2$) and specific oxides of nitrogen (iSNO$_x$) emissions as a function of SOI. iSCO$_2$ emissions varied based on the SOI value and injector location. However, iSCO$_2$ emissions were still 25% lower than from petroleum fueled engines [4]. It is worth noting iSCO$_2$ emissions are not corrected for the global warming potential of methane, which has shown to be up to 20 times greater than CO$_2$ [18]. iSNO$_x$ emissions were relatively constant, between 10-11.5g/kWhr for both fuel systems and SOI values.
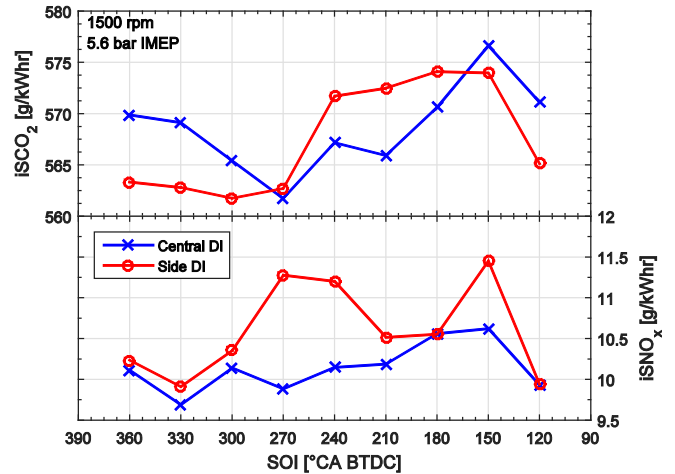

Figure 8: Specific CO2 and NOx Emissions as a function of SOI for Central and Side DI

EGR DILUTION TOLERNACE

EGR sweeps were performed for each injection system at three nominal SOI timings to determine the dilution tolerance for each system, as well as the effect of the induced charge motion from the gaseous injection event. Figure 9 shows that for SOI 300°CA BTDC, central and side DI cross the 3% limit at 6.5 and 5.4% EGR, respectively. Delaying the SOI to 240° CA BTDC helped to extend the dilution tolerance to 13.9 and 15.9% for central and side DI, respectively. A fully closed valve injection event led to

14.7 and 14.6% EGR tolerance for central and side DI, respectively. EGR dilution allowed for a 1% and 0.9% absolute increase in efficiency for central and side DI at SOI 300°CA BTDC. SOI 240°CA BTDC led to a 1.3 and 1.2% increase in ITE for central and side DI, from the baseline of 35.3 and 35.9%, respectively. Central DI led to a 0.9% increase in ITE from 34.5%, at SOI 120°CA BTDC. For a closed valve injection event, side DI has the highest efficiency improvement of 1.6% absolute from the 35.1% baseline. While there is similar dilution tolerance for SOI 300 and 120°CA BTDC for central and side DI, there is a 2% difference between the two injector locations at SOI 240°CA BTDC. As previously discussed, this is further indication side DI may help to improve the in-cylinder charge motion more than central DI, especially at SOI 240°CA BTDC.
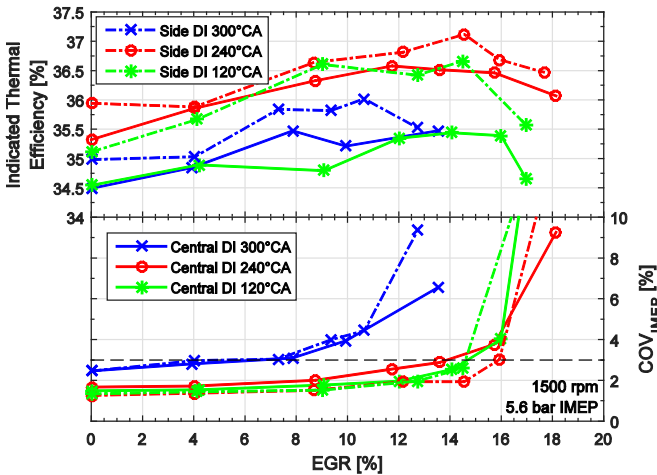

Figure 9: ITE and COVIMEP as a function of EGR for Central and Side DI

Flame development angle and combustion duration increase gradually with increasing EGR dilution, shown in Figure 10. Central and side DI at SOI 300°CA BTDC increase at the fastest rate. This is consistent with SOI 300°CA BTDC having the longest flame development angle and combustion duration at zero EGR operation. It is interesting to note the difference in flame development angle and combustion duration for central and side DI at SOI 240°CA BTDC. While this injection timing does lead to the highest efficiency for both injection systems, there are indications that central and side DI have different interactions with the intake air flow. A closed valve injection event for central and side DI led to the smallest increase in flame development angle and combustion duration. It is most interesting to note, central DI at SOI 120°CA BTDC closely resembles side DI at SOI 240°CA BTDC in terms of flame development angle and combustion duration, which is to be discussed in subsequent sections.
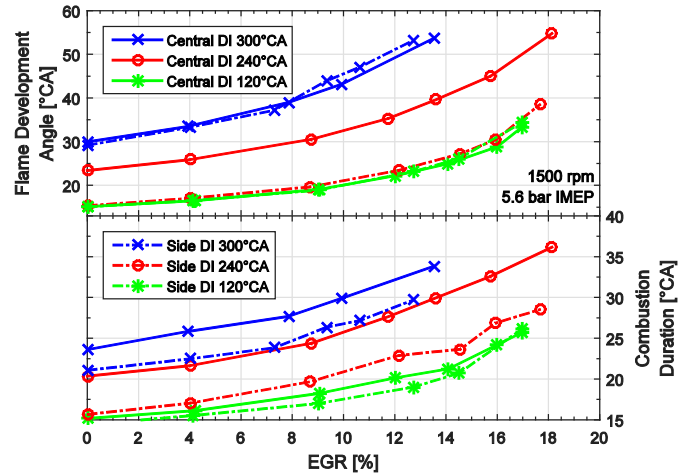

Figure 10: Flame Development Angle and Combustion Duration as a function of EGR for Central and Side DI

Figure 11 shows iSHC and iSCO emissions and combustion efficiency as a function of SOI for central and side DI. iSHC emissions remained relatively constant for both injection systems and all three injection timings. An increase in iSHC emissions was observed around the time each system reached the dilution tolerance limit. A general decrease in iSCO was also seen. While it would have been anticipated that iSCO would have increased with increasing EGR dilution due to incomplete combustion, combustion efficiency remained constant until the dilution tolerance limit and ITE kept increasing, partially due to the fact that there was less fuel bound carbon being introduced to the engine. In addition, as more EGR is introduced to the engine, in-cylinder pressure increases due to a higher trapped mass and temperatures decrease due to increasing diluent content. Literature has shown that when considering the equilibrium equation, $CO_2 = CO + 1/2 O_2$, the rate of CO formation decreases with increasing pressure and decreasing temperature [19].
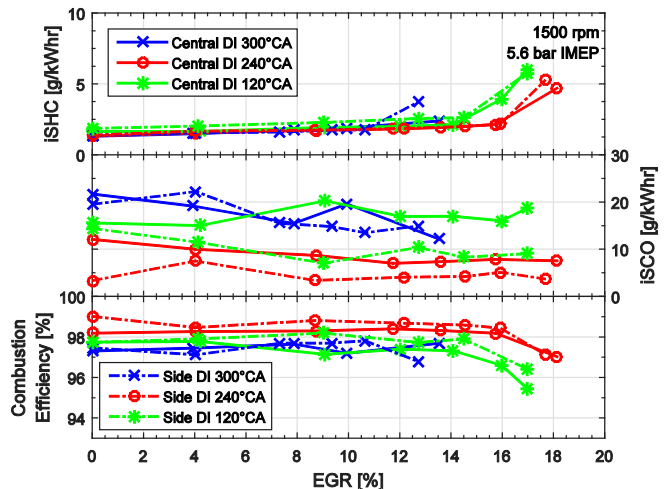

Figure 11: Specific HC and CO Emissions and Combustion Efficiency as a function of EGR for Central and Side DI

Figure 12 shows $iSCO_2$ and $iSNO_x$ emissions as a function of EGR for central and side DI. For the EGR sweep, $iSCO_2$ decreased due to ITE increasing with increasing EGR, holding engine load constant. At the same time, there was an 80% reduction in $iSNO_x$ for all conditions. Increased EGR, which acts as an in-cylinder diluent, leads to decreased in-cylinder temperatures helping to reduce the rate of the NO_x formation. iSNOx emissions decreased at the same rate for both injection systems and all injection timings.
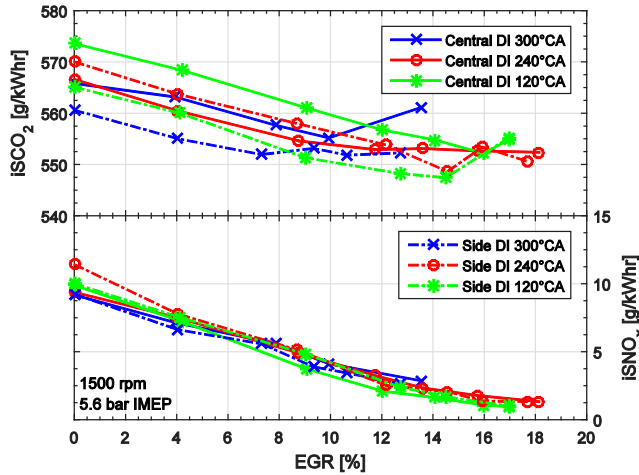

Figure 12: Specific CO₂ and NOx Emissions as a function of EGR for Central and Side DI

CFD RESULTS

To provide further understanding of the experimental data, CFD simulations of gas-exchange, fuel injection, and mixture formation process were performed to understand the impact of the gaseous injection event on the in-cylinder charge motion and stratification. Simulations were performed using the commercial CFD software CONVERGE. Previous works of the authors have focused on performing CFD simulations of mixture formation of the same engine, although for hydrogen DI and inward opening injectors [20,21]. More recently, CFD studies of mixture formation from the outward opening NG DI injector were performed and X-ray diagnostic techniques were used to validate simulation results [22].

Shown in Figure 13 is the in-cylinder tumble ratio for central and side DI at the three nominal SOI values. As seen, the tumble motion remains the same for all six cases from 360 to 300°CA BTDC, because injection has not yet occurred. At SOI 300°CA BTDC, the CFD simulation predicts that both central and side DI reverse the tumble flow during the gaseous injection event. This helps to explain why SOI 300°CA BTDC is a poor mixing point, given with the lowest ITE and EGR dilution tolerance. Delaying to SOI 240°CA BTDC, it can be seen that both central and side DI increase the tumble. However, the increase in tumble ratio is much larger for side DI as compared to central DI. This is due to the path of the gaseous jet, which at this SOI impinges on the side wall first and on the piston later, thus increasing tumble. It is worth noting that at earlier SOI, the side gaseous jet impinges

on the piston first, and this explains the reversed tumble. In general, central DI does not greatly affect in-cylinder tumble, due to a more neutral path of the injected gas, which does not significantly amplify or disrupt tumble. This similar trend of amplification and disruption of the tumble motion can be seen at SOI 120°CA BTDC with side and central DI, respectively.
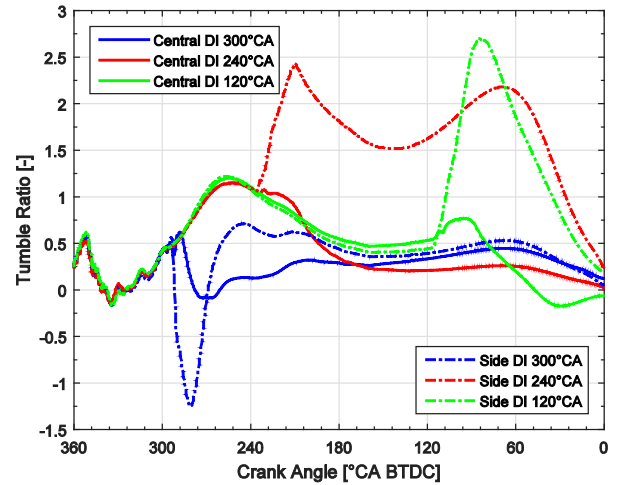

Figure 13: Global Tumble Ratio

Figure 14 shows the velocity field on the symmetry tumble plane for central and side DI with SOI 240°CA BTDC, at 60°CA BTDC, obtained by CFD calculations. While the spark timings for these given images could have been used, 60°CA BTDC was chosen to emphasize the different tumble properties during the compression stroke, also seen in Figure 13. For central DI, there is a weak tumble motion, which is generally damped out by the gaseous fuel injection that aims at the piston. Conversely, the tumble motion is much stronger for side DI, due to the gaseous jet induced velocity field that builds together with the intake flow. This is also seen in Figure 14 where the velocity magnitudes for side DI are considerably higher than central and a clear tumble motion within the cylinder can be seen. This helps to further reaffirm that injecting along the tumble motion, such is the case with side DI, promotes a stronger tumble motion within the cylinder [12].
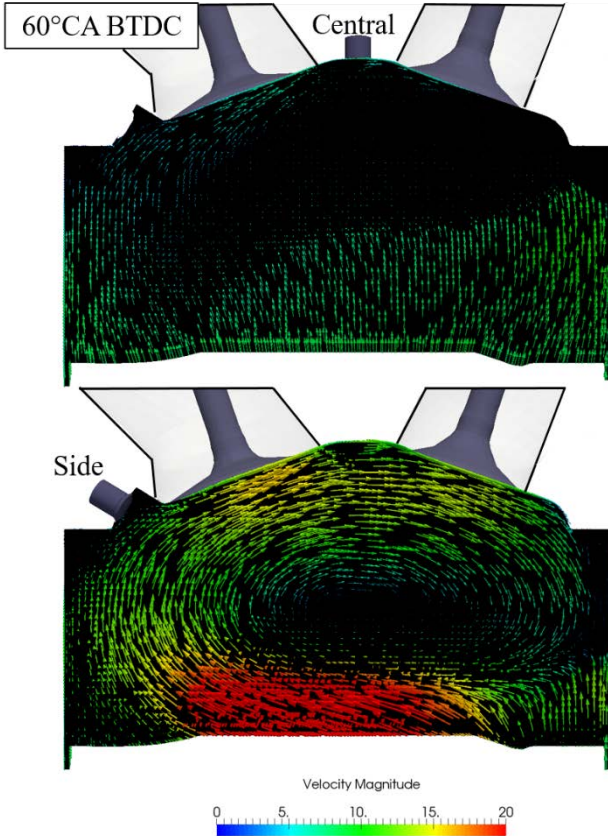
Figure 14: Velocity field for Central and Side DI with SOI 240°CA BTDC, at 60°CA BTDC

The average turbulent kinetic energy (TKE) value in the cylinder domain can be related back to the combustion duration. As seen in Figure 15, the TKE at the time of spark, indicated by the black square, is similar for both central and side DI at SOI 300°CA BTDC and SOI 240°CA BTDC for central DI. This agrees with Figure 5, where combustion duration for the three conditions are within 3°CA of each other. Globally, central DI has the highest TKE value at the time of ignition for SOI 120°CA BTDC. It is interesting to note that side DI at SOI 240 and 120°CA BTDC shows similar TKE values at the time of ignition. This is again consistent with Figure 5, where central and side DI at SOI 120°CA BTCD as well as side DI at SOI 240°CA BTDC show combustion duration within 1°CA. This is also consistent with results in Figure 10 where, the three conditions with a higher level of TKE show a combustion duration within 5°CA of each other for a given EGR rate. Therefore, side DI injection is more effective than central DI injection in enhancing in-cylinder tumble and turbulence, and this has a positive impact on both flame development angle and combustion duration.
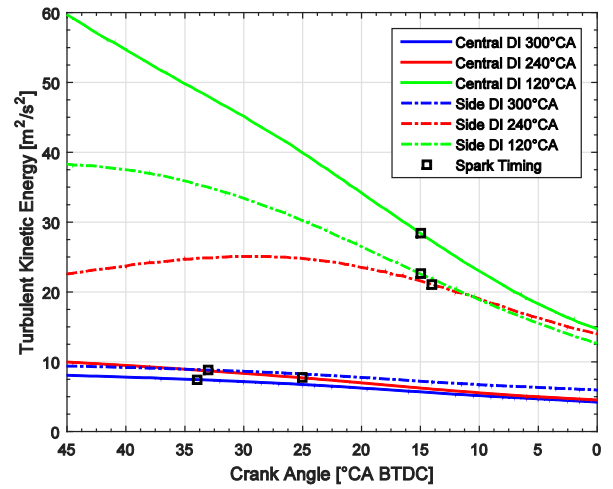

Figure 15: Global Turbulent Kinetic Energy

The standard deviation of the global relative air-fuel ratio, phi, throughout the cylinder, can be used as a measure of the degree of stratification. While the standard deviation of phi does not give an exact idea of where rich and lean zone are located in the combustion chamber, it can quantitatively describe the level of homogeneity throughout the combustion chamber, which has influence on the flame propagation process, ultimately having some impact on the ITE. At the time of spark, side DI at SOI 240°CA BTDC has the lowest standard deviation of phi, indicating the highest level of homogeneity. This aligns with Figure 4 and Figure 10, where side DI at SOI 240°CA BTDC has the highest ITE with and without EGR dilution. The standard deviation of phi is expected to increase when delaying from SOI 300 to 120°CA BTDC for both side and central DI, due to less time available for mixing prior to the spark event. However, it is interesting to observe that for both central and side DI, most effective mixing is achieved at SOI 240°CA BTDC, which matches the peak ITE in Figure 4.
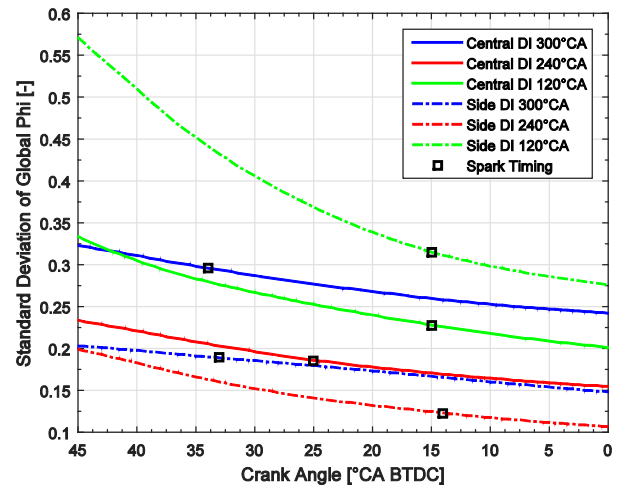

Figure 16: Global Standard Deviation of Phi

To further support the data shown in Figure 16, presented in Figure 17 is the phi distribution throughout the cylinder for central and side DI for SOI 120 and 240°CA BTDC, respectively. These images are captured at the spark timing for the given condition, and are provided to facilitate the understanding of the level of homogeneity throughout the cylinder. As can be seen, there is a rich region local to the injector for central DI at spark timing. This corresponds well to the data presented in Figure 16, where there is an increase level of inhomogeneity. Accordingly, there is a strong level of homogeneity within the cylinder for SOI 240°CA BTDC for side DI, shown in Figure 17.
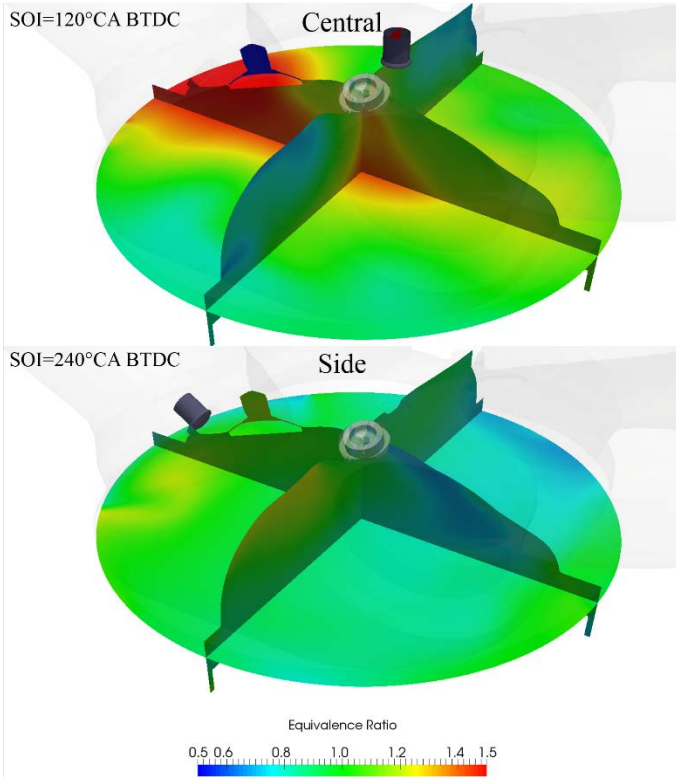

Figure 17: Phi distribution for Central and Side DI at Spark Timing

The CFD results show that there is a fundamental difference in the interaction of the gaseous injection with the intake flow for central and side DI. CFD calculations do not include combustion and are limited to the analysis of mixture formation as a means to interpret the engine data comprehensively. The experimental and numerical results shown indicate that a compromise between high turbulence and low stratification has to be reached. To this purpose, side DI proves to be the best injection location, and SOI 240°CA BTDC to be the best injection timing, by more effectively enhancing the interaction between the injected gas and the intake-induced flow with a consequent benefit in terms of engine efficiency.

CONCLUSION

A series of steady-state tests were performed at part-load conditions to assess the effects of a gaseous injection event on the combustion process as well as EGR dilution tolerance, for central and side mounted DI. Experimental results show that varying the SOI can dramatically reduce the flame development angle and combustion duration, as well as increase the ITE. In addition, the SOI had a direct impact on the dilution tolerance of both central and side DI. While early injection timings led to poor dilution tolerance, delaying the SOI to 240 and 120°CA BTDC, coinciding with maximum ITE and a closed-valve injection event, allowed for similar dilution tolerance. It was also shown that central and side mounted DI had a different response in terms of flame development angle and combustion duration for an EGR sweep. In addition, NG DI allowed for a 25% reduction in CO_2 emissions relative to gasoline operation. Side DI resulted in a general reduction iSCO emissions and an increased combustion efficiency; for some SOI values, side DI resulted in higher iSHC emissions. CFD results confirmed that side DI can help to amplify the tumble motion, while central DI has no significant effect. CFD simulation also helped to validate that the SOI can directly impact the in-cylinder charge motion due to the gaseous injection event. It has been shown that side DI with an intermediate SOI for this engine configuration has the strongest benefit to the combustion process. The results of the study have shown NG DI to be a viable option for a purpose built NG engine, especially in a part-load condition, where traditional methods of NG injection have led to poor levels of efficiency and dilution tolerance.

NOMENCLATURE

CFD	Computational fluid dynamics
CNG	Compressed natural gas
CO	Carbon monoxide
CO₂	Carbon dioxide
DI	Direct injection
EOI	End of injection
EVC	Exhaust valve close
EVO	Exhaust valve open
GDI	Gasoline direct injection
iS	Indicated specific
IVC	Intake valve close
IVO	Intake valve open
m_a	Mass of air
m_f	Mass of fuel
NG	Natural gas
NO$_x$	Oxides of nitrogen
PFI	Port-fuel injection
Q_{HVf}	Heating value of fuel
Q_{HVi}	Heating value of specie
SOI	Start of injection
THC	Total hydrocarbon
TKE	Turbulent kinetic energy
x_i	Mass fraction of specie

CONTACT INFORMATION

Thomas Wallner
Argonne National Laboratory
9700 South Cass Avenue
Lemont, IL 60439, USA
+001-630-252-3003
twallner@anl.gov

REFERENCES

[1] "Fuel for Thought." : The First Natural Gas Vehicles. N.p., n.d. Web. 22 Apr. 2016.

[2] "U.S. Energy Information Administration - EIA - Independent Statistics and Analysis." Short-Term Energy Outlook. N.p., n.d. Web. 22 Apr. 2016.

[3] "Fuel Prices." Alternative Fuels Data Center:. N.p., n.d. Web. 22 Apr. 2016.

[4] Weber, C., Kramer, U., Klein, R., "CNG-Specific Downsizing - Potentials and Challenges", Internationales Wiener Motorensymposium 2015.

[5] Bach, C., "CO2 Reduction and Cost Efficiency Potential of Natural Gas Hybrid Passenger Cars," SAE Int. J. Engines 4(2):2395-2404, 2011, doi:10.4271/2011-24-0110.

[6] Sevik, J., Pamminger, M., Wallner, T., Scarcelli, R. et al., "Performance, Efficiency and Emissions Assessment of Natural Gas Direct Injection compared to Gasoline and Natural Gas Port-Fuel Injection in an Automotive Engine," SAE Int. J. Engines 9(2):2016, doi:10.4271/2016-01-0806.

[7] Mispreuve L., Magere E., Kermarrec S., Obiols J., Delpech V., Soleri D., "Development and Potential of the Renault CNG 2.0L Turbocharged Engine", FISITA F2010-A-131.

[8] Delpech, V., Obiols, J., Soleri, D., Mispreuve, L. et al., "Towards an Innovative Combination of Natural Gas and Liquid Fuel Injection in Spark Ignition Engines," SAE Int. J. Fuels Lubr. 3(2):196-209, 2010, doi:10.4271/2010-01-1513.

[9] Anderson, J., Miers, S., Wallner, T., Stutenberg, K. et al., "Performance and Efficiency Assessment of a Production CNG Vehicle Compared to Its Gasoline Counterpart," SAE Technical Paper 2014-01-2694, 2014, doi:10.4271/2014-01-2694.

[10] Husted, H., Karl, G., Schilling, S.,Weber, C., "Direct Injection of CNG for Driving Performance with Low CO2," 23rd Aachen Colloquium Automobile and Engine Technology 2014.

[11] Husted, H., Karl, G., Schilling, S.,Weber, C., "Direct Injection of CNG for Driving Performance with Low CO2," 23rd Aachen Colloquium Automobile and Engine Technology 2014.

[12] Seboldt, D., Lejsek, D., Bargende, M., "Untersuchungen zum Einfluss von Einblasebeginn und Einblaserichtung auf die Gemischbildung und Verbrennung an einem $\lambda = 1$ betriebenen Ottomotor mit CNG-Direkteinblasung," 2015 IAV Conference.

[13] Van Alstine, D., Montgomery, D., Callahan, T., Florea, R., "ABILITY OF THE METHANE NUMBER INDEX OF A FUEL TO PREDICT RAPID COMBUSTION IN HEAVY DUTY DUAL FUEL ENGINES FOR NORTH AMERICAN LOCOMOTIVES", ASME ICEF 2015, ICEF2015-1119.

[14] Kubesh, J., King, S., and Liss, W., "Effect of Gas Composition on Octane Number of Natural Gas Fuels," SAE Technical Paper 922359, 1992, doi:10.4271/922359.

[15] Standard Test Method for Motor Octane Number of Spark-Ignition Engine Fuel, ASTM International D2700.

[16] "Fuel Quality Calculator." Cummins Westport. N.p., n.d. Web. 23 Oct. 2015.

[17] Heywood, J.B., "Internal Combustion Engine Fundamentals," McGraw-Hill Book.

[18] "Understanding Global Warming Potentials." US Environmental Protection Agency. N.p., n.d. Web. 18 Apr. 2016.

[19] "An introduction to combustion: concepts and applications," Stephen R.Turns - WCB/McGraw-Hill - 2000

[20] Scarcelli, R., Wallner, T., Salazar, V., and Kaiser, S., "Modeling and Experiments on Mixture Formation in a Hydrogen Direct-Injection Research Engine," SAE Int. J. Engines 2(2):530-541, 2010, doi:10.4271/2009-24-0083.

[21] Scarcelli, R., Wallner, T., Matthias, N., Salazar, V. et al., "Mixture Formation in Direct Injection Hydrogen Engines: CFD and Optical Analysis of Single- and Multi-Hole Nozzles," SAE Int. J. Engines 4(2):2361-2375, 2011, doi:10.4271/2011-24-0096.

[22] Bartolucci, L., Scarcelli, R., Wallner, T., Swantek, A. et al., "CFD and X-Ray Analysis of Gaseous Direct Injection from an Outward Opening Injector," SAE Technical Paper 2016-01-0850, 2016, doi:10.4271/2016-01-0850.